Nano Energy 28 (2016) 390–396

Contents lists available at ScienceDirect

Nano Energy

journal homepage: www.elsevier.com/locate/nanoen

Towards visible-light water splitting Photocatalysts: Band engineering of two-dimensional $A_5B_4O_{15}$ perovskites

Dihua Wu, Xu Zhang, Yu Jing, Xudong Zhao, Zhen Zhou *

Tianjin Key Laboratory of Metal and Molecule Based Material Chemistry, Computational Centre for Molecular Science, Institute of New Energy Material Chemistry, Collaborative Innovation Center of Chemical Science and Engineering (Tianjin), School of Materials Science and Engineering, National Institute for Advanced Materials, Nankai University, Tianjin 300350, PR China

ARTICLE INFO

Article history:
Received 7 January 2016
Received in revised form
26 May 2016
Accepted 31 August 2016
Available online 31 August 2016

Keywords:
Perovskite
Photocatalytic water splitting
2D materials
Band engineering

ABSTRACT

Photocatalytic water splitting is a promising route to achieve renewable hydrogen production. In this work, a series of $A_5B_4O_{15}$ (A=Ca, Sr, Ba; B=V, Nb, Ta) layered perovskite materials, were investigated through density functional theory computations. We revealed that changing B ions can modify the band gap, and A-ion substitution can tune the band-edge position. Therefore, through A/B ion combination, we can realize the band engineering of $A_5B_4O_{15}$ materials. Electron/hole effective mass and water adsorption of $A_5B_4O_{15}$ materials were also explored. Further investigations suggest that $Ca_5V_4O_{15}$ nanosheet, with an appropriate band gap and an optimal band-edge position, would be a promising photocatalyst for visible-light water splitting.

1. Introduction

Photocatalytic water splitting has attracted tremendous attention as a potential route to address energy and environment related issues [1,2]. Since the first realization of water splitting without any applied electric power by Fujishima and Honda [3], significant breakthrough has emerged to boost the performance [4–7]. However, currently most industrial hydrogen is still produced from fossil fuels, and present photocatalytic systems are not economical for industrial hydrogen production [8]. The absence of stable photocatalysts that can operate under visible light with high efficiency is a critical obstacle for commercial photocatalytic water splitting [9,10].

Perovskite materials stand out as promising photocatalysts for water splitting [8,11–13]. The high stability of perovskite-like structures enables myriad A- and B-site ion combinations, and offers enormous flexibility for performance optimization [12]. For example, water splitting activity was found in $ATaO_3$ (A=Li, Na, and K) [14], $Sr_2M_2O_7$ (M=Nb and Ta) [15], $A_mB_mO_{3m+2}$ (m=4, 5; A=Ca, Sr, La; B=Nb, Ti) [16], and $A_{2-x}La_2Ti_{3-x}Nb_xO_{10}$ (A=K, Rb, Cs; x=0, 0.5, 1) [17]; visible-light-driven photocatalytic performances were also observed in $NaBiO_3$ [18], Cu(II)-$(Sr_{1-y}Na_y)(Ti_{1-x}Mo_x)O_3$ [19], and $(Ag_{0.75}Sr_{0.25})(Nb_{0.75}Ti_{0.25})O_3$ [20].

As layered perovskite materials with B-site vacancies [21,22], $A_5B_4O_{15}$ is of particular interest as water splitting photocatalysts. In 2005, water splitting activity was found for both $Sr_5Ta_4O_{15}$ [23] and $Ba_5Ta_4O_{15}$ [24]. Later, a quantum yield as high as 17% was achieved for $NiO_x/Ba_5Nb_4O_{15}$ by Miseki et al., who systematically investigated $A_5Nb_4O_{15}$ (A=Sr, Ba), and $ALa_4Ti_4O_{15}$ (A=Ca, Sr, Ba) [25,26]. By comparison, the quantum yield of nanocrystalline TiO_2 is 16% [27]. Further, the H_2 production rate was improved in $Ba_5Ta_4O_{15}$ with 0.2 wt% nitrogen doping, due to the enhanced visible light absorbance [28]. Chen et al. revealed that H_2 evolution on $Pt/Sr_5Ta_4O_{15-x}N_x$ and O_2 evolution on $CoO_x/Sr_5Ta_4O_{15-x}N_x$ under visible light irradiation [29]. Enhanced photocatalytic activity for $BaLa_4Ti_4O_{15}$ was reported by Negishi et al. [30,31] by loading ultra-small gold clusters. Li et al., proposed that P–Mo co-doped $Ba_5Nb_4O_{15}$ could own visible light activity [32]. Experimentally, Marschall et al. [33] prepared $Ba_5Ta_4O_{15}$, $Ba_5Ta_2Nb_2O_{15}$ and $Ba_5Nb_4O_{15}$ nanofibers and demonstrated their ability to generate hydrogen without cocatalysts.

The realization of two-dimensional (2D) nanosheet morphology, which shows several advantages as water splitting photocatalysts [9,34–37], is feasible for $A_5B_4O_{15}$ materials due to the layered structure. Zhu et al. [38] reported that $Ba_5Ta_4O_{15}$ monolayers prepared through a hydrothermal route under low temperatures without templates exhibited better photocatalytic performance than the bulk. Park et al. investigated the H_2 evolution on bulk $Ba_5Nb_4O_{15}$, $Ba_5Nb_4O_{15}$ nanosheets with ~30 nm thickness and $Ba_5Nb_4O_{15}$ nanosheets with ~6 nm thickness, and revealed that the water splitting activity increased with decreasing the

* Corresponding author.
E-mail address: zhouzhen@nankai.edu.cn (Z. Zhou).

http://dx.doi.org/10.1016/j.nanoen.2016.08.064
2211-2855/

nanosheet thickness [39]. The reduced physical dimension facilitates the diffusion of electron/hole to the surface to participate the photocatalytic reaction; therefore, 2D materials generally shows lower electron-hole recombination rate than their bulk counterparts [40]. Also, 2D nanosheets have much larger surface areas that could promote the adsorption of H_2O, H^+ and OH^- [34].

$A_5B_4O_{15}$ materials have versatile structures of perovskites and can also be fabricated into monolayer nanosheets, which makes them rather promising as water splitting photocatalysts. However, few studies have been performed on the electronic structure of $A_5B_4O_{15}$ and several questions remain open. For example, how would A/B ions influence the electronic structure and how would quantum confinement effect modify the band gap of $A_5B_4O_{15}$? Does the material possess visible light absorption capability? Especially, the band edge positions of $A_5B_4O_{15}$, which are critical for photocatalysts, are unexplored. In this work, we systematically investigated the electronic properties of $A_5B_4O_{15}$ (A=Ca, Sr, Ba; B=V, Nb, Ta) bulks and nanosheets through density functional theory (DFT) computations. The lattice parameters and band structures between bulk and nanosheets were compared to illustrate their relation. The influence of changing A/B ions on band gap and band edge position was investigated, as well as effective mass and water adsorption. In light of these analyses, we predicted that $Ca_5V_4O_{15}$ nanosheets are promising visible light photocatalysts for water splitting.

2. Computational details

All DFT computations were performed by using projector augmented wave (PAW) [41] method as implemented in Vienna *ab initio* simulation package (VASP) [42]. Lattice parameters and atomic coordinates were optimized with generalized gradient approximation (GGA) as implemented by Perdew, Burke and Ernzerhof (PBE) [43]. Spin polarization and plane-wave energy cutoff of 550 eV were employed for all computations. Spin-orbital coupling shows trivial influence on band gaps; therefore, it is not adopted in our computations. HSE06 hybrid functional [44,45] was applied for the computation of band edge positions and accurate band gaps. K-point separation of 0.025 $Å^{-1}$ for PBE calculations and 0.04 $Å^{-1}$ for expensive HSE06 computations was employed. The band edge position relative to the vacuum level was evaluated by electrostatic potential alignments. For the calculations of convex hull, a correction scheme of formation enthalpy proposed by Jain et al. [46] was adopted. Effective mass for both electrons and holes was evaluated through the equation:

$$m^* = \hbar^2\left(\frac{d^2E}{dk^2}\right)^{-1}$$

The calculated effective mass was represented in the unit of m_0 (electron rest mass). For the calculation of water adsorption, $2 \times 2 \times 1$ supercells and Monkhorst-Pack grids of $3 \times 3 \times 1$ k-points were adopted for nanosheets.

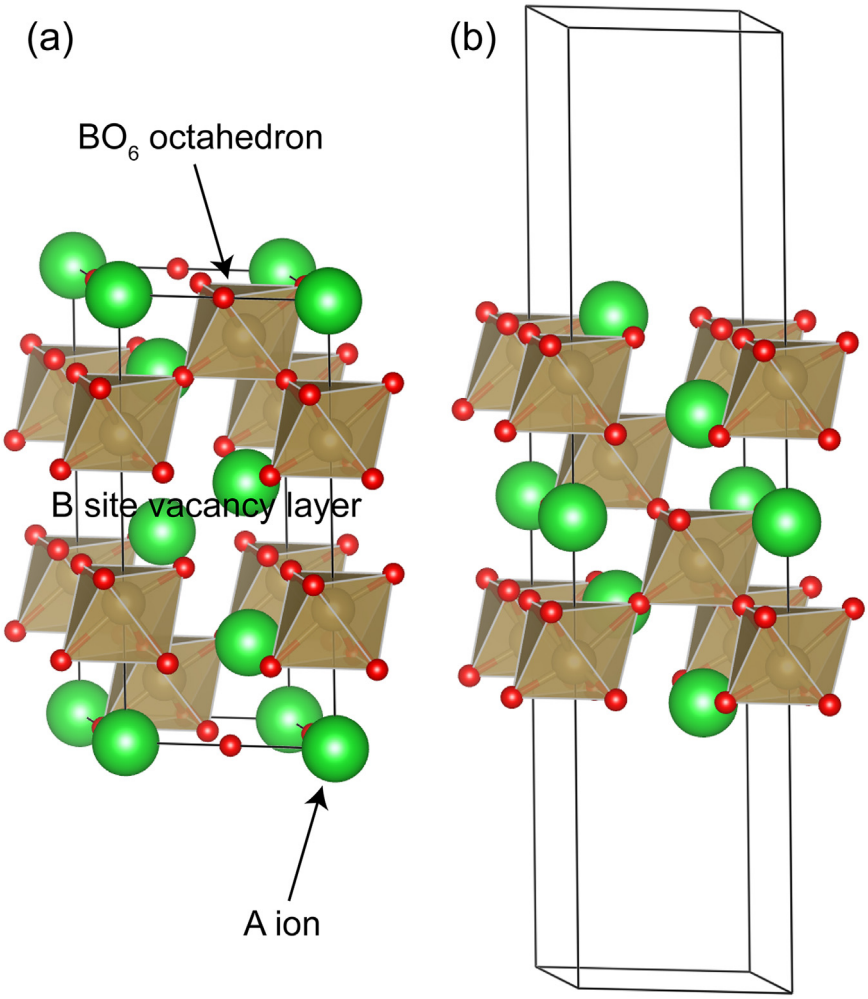

Fig. 1. Crystal structures of $A_5B_4O_{15}$ (a) bulk and (b) nanosheet.

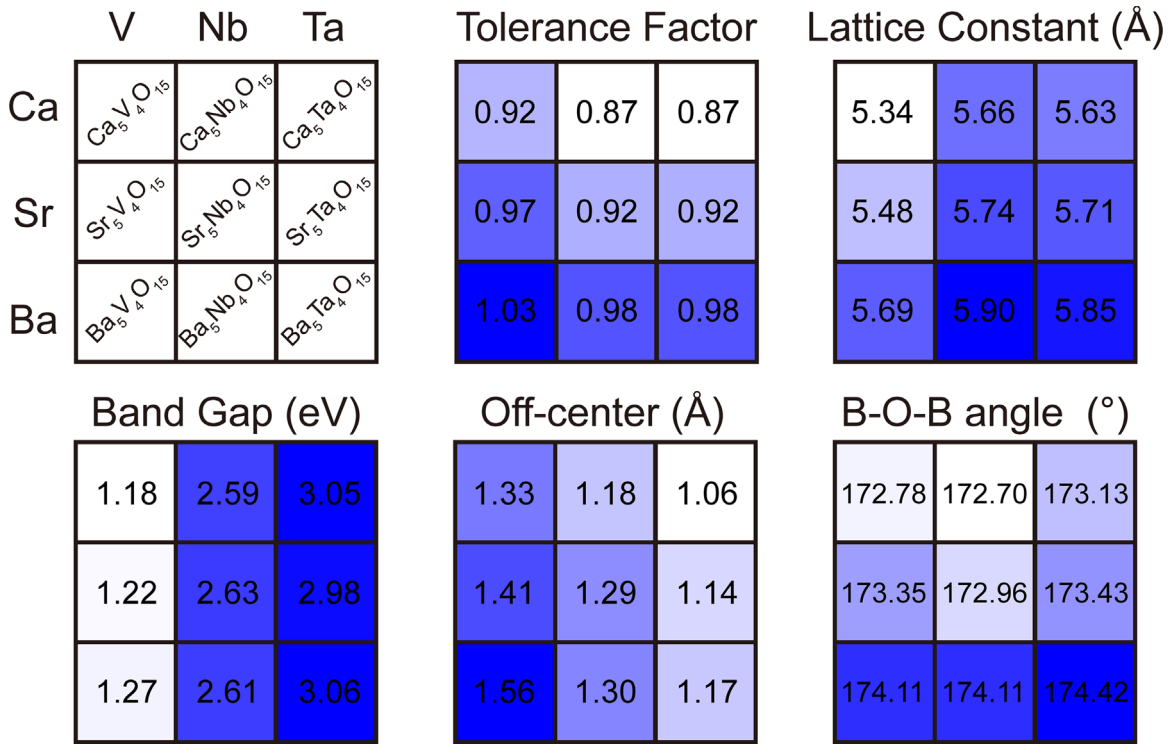

Fig. 2. Color map of tolerance factor, lattice constant, band gap, average B ion off-center value and average B-O-B angle of $A_5B_4O_{15}$. The evaluation method for B ion off-center value is presented in Fig. S1.

3. Results and discussion

$A_5B_4O_{15}$ has B-site vacancies compared with ABO_3 perovskites as shown in Fig. 1a. For $A_5B_4O_{15}$ nanosheets, at least 15-Å vacuum space was inserted between layers to avoid artificial interactions (Fig. 1b). For perovskite materials, due to their geometrical configurations, there is a relationship between the ionic radii of A, B and O, which is represented as tolerance factor (t) by Goldschmidt [47]. The tolerance factor is defined by the following equation:

$$t = (r_A + r_O)/\sqrt{2}(r_B + r_O)$$

generally, perovskite structures satisfy t=0.7–1.1 [48]. As shown in Fig. 2, all investigated structures satisfy the restriction mentioned above. Lattice constants (a) are also presented in Fig. 2. For A ions, heavier elements have larger lattice constants because of their larger radii. For B ions, V has the smallest lattice constant; due to lanthanide contraction, Nb and Ta have almost the same radius [49]; therefore, the corresponding structures also show similar lattice constant.

Clearly, compared with A ion, B ion is the major influential factor for band gap variation (Fig. 2). Larger electronegativity difference between B ion and oxygen leads to larger band gap [50]. The electronegativity decreases from V (1.63) to Nb (1.6) to Ta (1.5); therefore, the band gap increases from V to Ta. A ion also has influence on band gap [51]. Previous investigations demonstrated that, larger B off-center enlarges the band gap [50], and with the B-O-B angle closer to 180°, the band gap decreases [48,52,53]. Our results demonstrate that, with larger radius of A ion, B ion is more off-center, but the B-O-B angle becomes closer to 180°. Therefore, the influence of A ion on the band gap becomes ambiguous because of the above two reverse factors. Note that the band gap of $Ba_5Nb_4O_{15}$ is also slightly smaller than that of $Sr_5Nb_4O_{15}$ in experiments [26], in agreement with our results.

The partial density of states (PDOS) of A and B ions is shown in Fig. 3; the valence band maximum (VBM) of all $A_5B_4O_{15}$ materials is dominated by the p orbital of oxygen, and the conduction band minimum (CBM) consists of d orbital of B ion and p orbital of oxygen. Previous studies on $Sr_2Ta_2O_7$ and $Sr_2Nb_2O_7$ show that 4p orbital of Sr contributes to the VBM [54,55]. Our results demonstrate that $A_5B_4O_{15}$ shows different behaviors, since A ion does not contribute to either VBM or CBM. The consequence is also straightforward; the choice of B ion has obvious influence on band gaps, while A ion only has marginal influence. The band gap increases as B ion changes from V to Ta, in agreement with previous experimental results, which demonstrate that $Ba_5Nb_4O_{15}$ has smaller band gap than $Ba_5Ta_4O_{15}$ [33].

Unlike other 2D materials, several properties of $A_5B_4O_{15}$ nanosheets are surprisingly similar to those of their bulk counterparts. All lattice constants (Table 1) only have $<1\%$ deviation compared with bulk structures. The formation energy of nanosheets, which is defined as the energy difference between nanosheets and bulks per formula, was also calculated. For comparison, the formation energy of experimentally available $Ba_5Ta_4O_{15}$ nanosheets is 2.00 eV [38]. Therefore, the synthesis of $Ca_5V_4O_{15}$, $Sr_5V_4O_{15}$, $Sr_5Ta_4O_{15}$, $Ba_5V_4O_{15}$ and $Ba_5Nb_4O_{15}$ nanosheets should be feasible, because they have lower formation energies than $Ba_5Ta_4O_{15}$ nanosheets, while the synthesis of $Ca_5Nb_4O_{15}$, $Ca_5Ta_4O_{15}$ and $Sr_5Nb_4O_{15}$ nanosheets might be difficult due to the strong interlayer interaction.

The band gap of $A_5B_4O_{15}$ nanosheets is quite close to that of the bulk material. Certain nanosheets even have slightly smaller band gaps (Fig. S5), such as $Ba_5Ta_4O_{15}$, which also experimentally shows smaller band gap in its nanosheet form [38]. The results contradict to the general observation that the quantum confinement effect enlarges band gaps. To further illustrate the band gap difference between bulks and nanosheets, the charge density of VBM and CBM of bulk $Sr_5Nb_4O_{15}$ was calculated and is shown in Fig. 4a. The CBM consists of d_z^2 orbital of Sr and 2p orbital of O, and the VBM is mainly contributed by the 2p orbital of O. The results are in agreement with the PDOS calculations (The DOS and band structures of nanosheets are all shown in Figs. S2–S4). Both CBM and

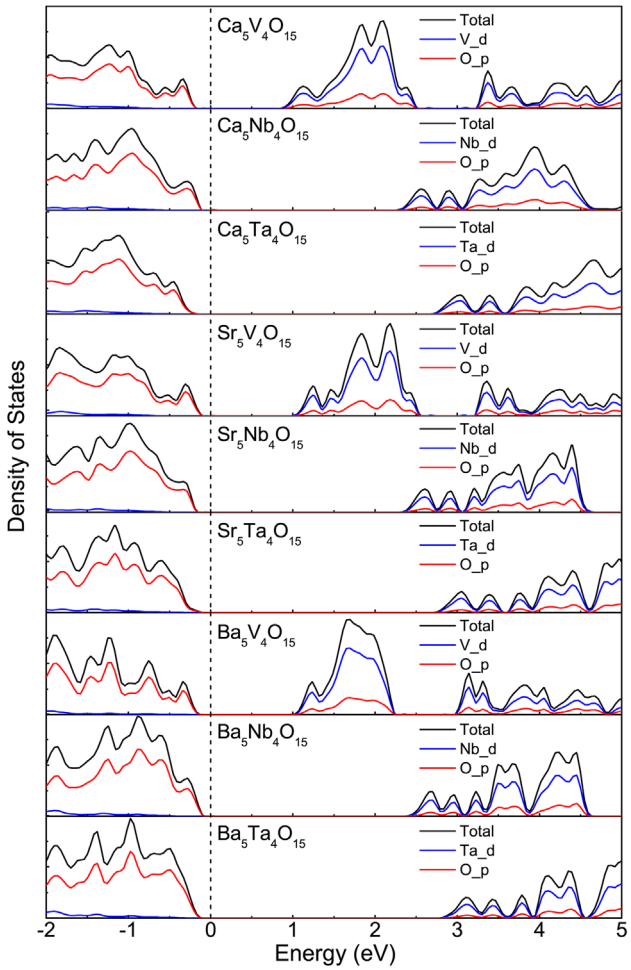

Fig. 3. DOS of $A_5B_4O_{15}$ materials (A=Ca, Sr, Ba; B=V, Nb, Ta), in which black lines are the total DOS, blue lines are *d* orbital of B ions and red lines are *p* orbital of oxygen. Fermi levels are set to zero and denoted with dashed lines.

Table 1
Formation energies, lattice constants and band gaps of $A_5B_4O_{15}$ nanosheets.

Nanosheet	Lattice constant (Å)	Formation energy (eV)	Band gap (eV)
$Ca_5V_4O_{15}$	5.305	1.80	1.14
$Ca_5Nb_4O_{15}$	5.623	3.14	2.40
$Ca_5Ta_4O_{15}$	5.593	3.38	2.85
$Sr_5V_4O_{15}$	5.454	1.54	1.25
$Sr_5Nb_4O_{15}$	5.740	2.62	2.46
$Sr_5Ta_4O_{15}$	5.684	1.92	2.83
$Ba_5V_4O_{15}$	5.651	1.11	1.31
$Ba_5Nb_4O_{15}$	5.890	1.93	2.54
$Ba_5Ta_4O_{15}$	5.855	2.00	2.89

VBM show no obvious covalent interaction between layers. Also, the nearly flat conduction and valence bands in Γ-A of bulk $Sr_5Nb_4O_{15}$ indicate strong wavefunction localization; thus, similar band structures are observed in nanosheet (Fig. 4b) and bulk (Fig. 4c) forms.

Band edge positions are critical factors for photocatalysts. To obtain accurate VBM and CBM positions of $A_5B_4O_{15}$, HSE06 hybrid functional was adopted. $Ca_5Nb_4O_{15}$, $Sr_5Nb_4O_{15}$, $Ba_5Nb_4O_{15}$, $Ba_5V_4O_{15}$ and $Ba_5Ta_4O_{15}$ nanosheets were considered first to reveal the influence of A and B ions. As shown in Fig. 5, the calculated band gap and band edge position of single-layer MoS_2 is in good agreement with previous investigations [56]. The experimentally measured band gap for bulk $Ba_5Nb_4O_{15}$ is 3.9 eV [33], and our calculated band gap for the nanosheet is 3.78 eV; several experimentally estimated band gaps of bulk $Ba_5Ta_4O_{15}$ have been reported, including 3.9 eV [24], 4.1 eV [38], and 4.5 eV [33], and our calculated band gap for $Ba_5Ta_4O_{15}$ nanosheet is 4.11 eV. The calculated HSE06 band gaps are in good agreement with experimental results (Detailed band structures are shown in Fig. S6). The trend of band gaps revealed by HSE06 further confirmed the results of PBE calculations: A ion only has slight influence on the band gap, while the band gap increases with changing B ion from V to Ta.

However, for band edge positions, by comparing $Ca_5Nb_4O_{15}$, $Sr_5Nb_4O_{15}$ and $Ba_5Nb_4O_{15}$, we found that the band edge position shifts upward when A ion changes from Ca to Ba. The results are rather intriguing, since DOS calculations show that the PDOS of A ion do not contribute to either VBM or CBM. Previous theoretical investigations revealed that work function decreases with lattice elongation [57]. In our computations, different ionic radii of alkali earth elements lead to different lattice constants. Lattice constants increase from $Ca_5Nb_4O_{15}$ (5.623 Å) to $Sr_5Nb_4O_{15}$ (5.746 Å) and $Ba_5Nb_4O_{15}$ (5.892 Å), and work function decreases accordingly. For B ions, Nb shows lower CBM and VBM than Ta, while V shows lower CBM but higher VBM than Nb.

Inspired by these results, we further investigated the properties of $Ca_5V_4O_{15}$ nanosheets. The choice of V can reduce the band gap to visible light region, and the choice of Ca can lower band edge positions when compared with $Ba_5V_4O_{15}$ nanosheets. Fig. 5 shows that the band edge positions of $Ca_5V_4O_{15}$ nanosheets straddle H^+/H_2 and O_2/H_2O with a moderate band gap of 2.24 eV, which demonstrates its ability to generate both H_2 and O_2 within visible light region. Moreover, we investigated the thermodynamic properties of $Ca_5V_4O_{15}$ in Ca-V-O phase diagram, as shown in Fig. 6. The formation energy of bulk $Ca_5V_4O_{15}$ is 127 meV/atom above the hull. For comparison, the formation energy of diamond is 136 meV/atom above the hull [58]. Still, the high formation energy indicates that the synthesis of $Ca_5V_4O_{15}$ might be challenging. $Ba_5Ta_4O_{15}$ nanosheets have been successfully prepared by low-temperature hydrothermal method [38]; therefore, we suggest that bottom-up method would be a feasible routine to prepare $Ca_5V_4O_{15}$ nanosheets.

Effective masses for both electrons and holes of $A_5B_4O_{15}$ materials are summarized in Table 2. Even though certain trend can be observed in Table 2, for example, smaller A ion leads to reduced effective mass of both electrons and holes; however, all $A_5B_4O_{15}$ materials manifest heavy electron/hole effective mass. The calculated effective mass is comparable to that of $NaTaO_3$, in which the effective mass of both electrons and holes is about 8 m_0 [59]. Therefore, we propose that it is necessary to synthesize materials with small particle sizes for performance optimization. For layered materials like $A_5B_4O_{15}$, the ideal morphology should be 2D nanosheets [38,39].

Water adsorption was further investigated to understand the interaction between water and $A_5B_4O_{15}$ nanosheets. Three adsorption positions were considered (Fig. 7), and the adsorption energy was calculated through the following equation:

$$E_{ad} = E_{water-A_5B_4O_{15}} - E_{A_5B_4O_{15}} - E_{water}$$

where $E_{water-A_5B_4O_{15}}$, $E_{A_5B_4O_{15}}$ and E_{water} are the total energy of $A_5B_4O_{15}$ nanosheet with adsorbed water, pristine $A_5B_4O_{15}$ nanosheet and a single water molecule, respectively. The largest adsorption energies are found in Position A. Also, for Position A, the distance between water and the nanosheet is the shortest (Fig. 7). It is also observed that water adsorption at Position O for $Ba_5Ta_4O_{15}$ and Position B for $Ca_5Nb_4O_{15}$ is not stable, and water would migrate to Position A spontaneously, which further confirms the stronger water binding at Position A. The interaction

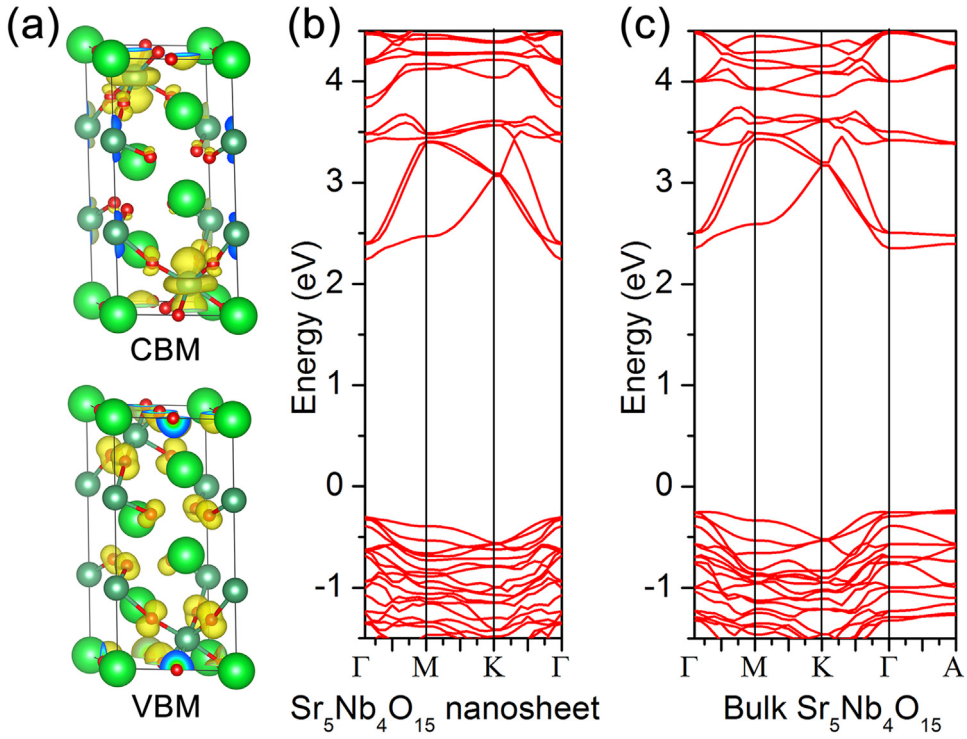

Fig. 4. (a) Charge density of CBM and VBM of bulk $Sr_5Nb_4O_{15}$ and band structures of (b) $Sr_5Nb_4O_{15}$ nanosheet and (c) bulk $Sr_5Nb_4O_{15}$.

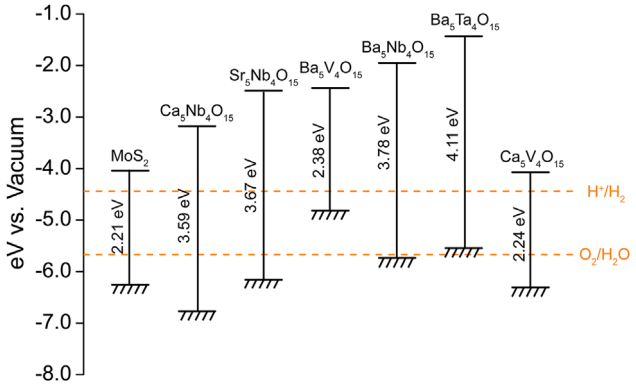

Fig. 5. VBM and CBM positions of various nanosheets. Redox potentials of H^+/H_2 and O_2/H_2O are represented by orange dash lines.

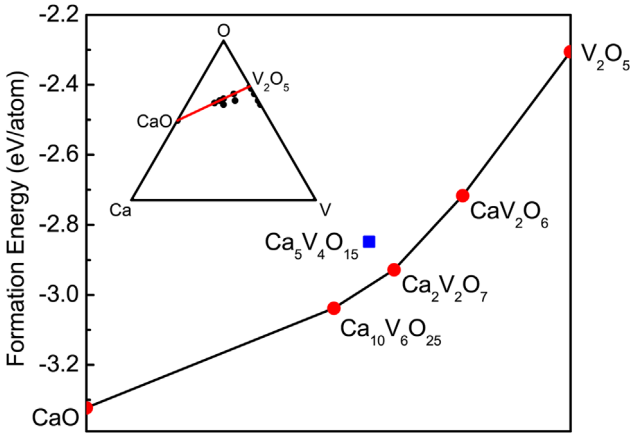

Fig. 6. Convex hull of Ca-V-O system from CaO to V_2O_5 (red line in the Ca-V-O phase diagram). Stable phases are obtained from Material Project [58].

Table 2
Calculated water adsorption energy and effective mass of electron/hole for $A_5B_4O_{15}$ nanosheets.

Nanosheets	Effective mass of electron (m_0)		Effective mass of hole (m_0)		Water adsorption energy (eV)		
	Γ-M	Γ-K	Γ-M	Γ-K	A	B	O
$Ca_5V_4O_{15}$	10.31	10.60	13.64	13.59	−1.08	−0.14	−0.10
$Ca_5Nb_4O_{15}$	8.71	8.74	13.64	13.62	−3.18	unstable	−1.24
$Ca_5Ta_4O_{15}$	9.12	8.63	12.46	12.46	−2.07	−0.17	−0.18
$Sr_5V_4O_{15}$	11.59	11.83	18.86	17.48	−0.63	−0.13	−0.11
$Sr_5Nb_4O_{15}$	8.61	7.77	14.78	14.24	−0.76	−0.68	−0.47
$Sr_5Ta_4O_{15}$	7.85	7.97	13.02	13.11	−1.56	−1.50	−1.25
$Ba_5V_4O_{15}$	14.12	14.40	60.52	43.78	−0.61	−0.28	−0.50
$Ba_5Nb_4O_{15}$	9.66	9.48	16.60	18.99	−0.85	−0.21	−0.17
$Ba_5Ta_4O_{15}$	8.05	7.95	14.54	14.26	−0.90	−0.73	unstable

between A ion and oxygen of water should be the main reason for the strong adsorption. Since the Coulomb interaction of Ca-O is stronger than that of Nb-O and Ta-O due to the smaller ionic radius of Ca, $Ca_5B_4O_{15}$ exhibits stronger adsorption for water, which could benefit for higher catalytic activity. Note that, in order to gain comprehensive insights into catalytic performances, further experimental investigations, such as charge transfer rate between water and the nanosheet, quantum yield and reaction mechanism, are required.

4. Conclusions

In conclusion, for $A_5B_4O_{15}$ materials, changing A ion only has trivial influence on the band gap, and band gap becomes larger when changing B ion from V to Ta. DOS analysis shows that the VBM of $A_5B_4O_{15}$ is mainly contributed by 2*p* orbital of O, and the CBM consists of *d* orbital of B ion and 2*p* orbital of O. Bulk $A_5B_4O_{15}$ and the nanosheet counterpart show similar band gaps. HSE

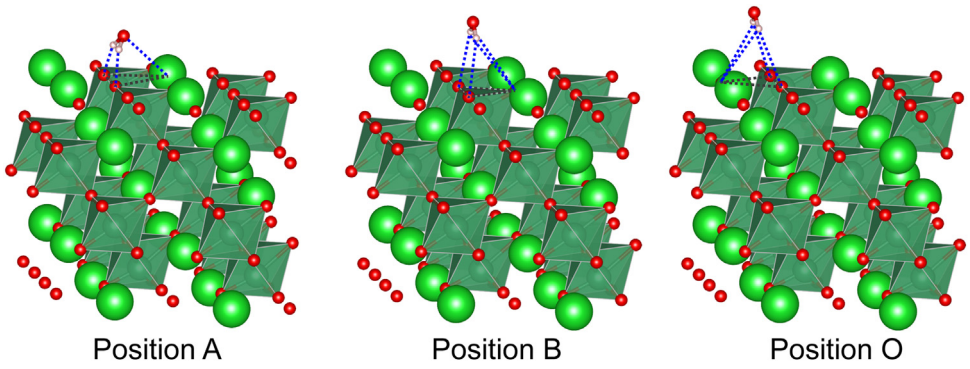

Fig. 7. Three positions for water adsorption. Gray triangles are drawn to indicate the adsorption position, and blue dot lines to indicate assumed interaction. Position A: hydrogen interacts with two oxygen in the surface and oxygen of water interacts with A ion. Position B: hydrogen interacts with oxygen atoms from one BO_6 octahedron. Position O: hydrogen interacts with oxygen atoms from three BO_6 octahedrons.

calculations revealed that the band edge position shifts upward when A ion changes from Ca to Ba, even though it only has trivial impact on the band gap. Our results demonstrate that the band engineering of $A_5B_4O_{15}$ materials is possible by A/B ion combination. Inspired by these results, we predict that $Ca_5V_4O_{15}$ nanosheet is a potential visible-light water splitting photocatalyst, with appropriate band gap and optimal band edge position. Thermodynamic analyses suggest that it is preferable to prepare $Ca_5V_4O_{15}$ nanosheets through bottom-up routes. The effective mass evaluation indicates that 2D nanosheets morphology is desirable for performance optimization. Computations also indicate that $Ca_5B_4O_{15}$ displays stronger binding for water. Our investigations pave the way for the realization of $A_5B_4O_{15}$ visible-light water splitting photocatalysts, and further experimental investigations are welcome to confirm the prediction.

Acknowledgements

This work was supported by NSFC (21273118 and 21421001) and MOE Innovation Team (IRT13022) in China. The computations were performed on Magic Cube at Shanghai Supercomputer Center.

Appendix A. Supporting information

Supplementary data associated with this article can be found in the online version at http://dx.doi.org/10.1016/j.nanoen.2016.08.064.

References

[1] K. Maeda, K. Teramura, D. Lu, T. Takata, N. Saito, Y. Inoue, K. Domen, Nature 440 (2006), 295-295.
[2] S.Y. Reece, J.A. Hamel, K. Sung, T.D. Jarvi, A.J. Esswein, J.J.H. Pijpers, D.G. Nocera, Science 334 (2011) 645–648.
[3] A. Fujishima, K. Honda, Nature 238 (1972) 37–38.
[4] Y. Tachibana, L. Vayssieres, J.R. Durrant, Nat. Photonics 6 (2012) 511–518.
[5] K. Sayama, K. Mukasa, R. Abe, Y. Abe, H. Arakawa, J. Photochem. Photobiol. A 148 (2002) 71–77.
[6] H. Kato, M. Hori, R. Konta, Y. Shimodaira, A. Kudo, Chem. Lett. 33 (2004) 1348–1349.
[7] J. Yang, D. Wang, H. Han, C. Li, Acc. Chem. Res. 46 (2013) 1900–1909.
[8] A. Kudo, Y. Miseki, Chem. Soc. Rev. 38 (2009) 253–278.
[9] A.K. Singh, K. Mathew, H.L. Zhuang, R.G. Hennig, J. Phys. Chem. Lett. 6 (2015) 1087–1098.
[10] X. Zhang, X.D. Zhao, D.H. Wu, Y. Jing, Z. Zhou, Adv. Sci. (2016), http://dx.doi.org/10.1002/advs.201600062.
[11] F.E. Osterloh, Chem. Mater. 20 (2008) 35–54.
[12] A. Kubacka, M. Fernández-García, G. Colón, Chem. Rev. 112 (2012) 1555–1614.
[13] X. Chen, S. Shen, L. Guo, S.S. Mao, Chem. Rev. 110 (2010) 6503–6570.
[14] H. Kato, A. Kudo, J. Phys. Chem. B 105 (2001) 4285–4292.
[15] A. Kudo, H. Kato, S. Nakagawa, J. Phys. Chem. B 104 (2000) 571–575.
[16] H.G. Kim, D.W. Hwang, J. Kim, Y.G. Kim, J.S. Lee, Chem. Commun. 12 (1999) 1077–1078.
[17] T. Takata, Y. Furumi, K. Shinohara, A. Tanaka, M. Hara, J.N. Kondo, K. Domen, Chem. Mater. 9 (1997) 1063–1064.
[18] T. Kako, Z. Zou, M. Katagiri, J. Ye, Chem. Mater. 19 (2007) 198–202.
[19] X. Qiu, M. Miyauchi, H. Yu, H. Irie, K. Hashimoto, J. Am. Chem. Soc. 132 (2010) 15259–15267.
[20] D. Wang, T. Kako, J. Ye, J. Am. Chem. Soc. 130 (2008) 2724–2725.
[21] M.A. Peña, J.L.G. Fierro, Chem. Rev. 101 (2001) 1981–2018.
[22] I.N. Jawahar, P. Mohanan, M.T. Sebastian, Mater. Lett. 57 (2003) 4043–4048.
[23] K. Yoshioka, V. Petrykin, M. Kakihana, H. Kato, A. Kudo, J. Catal. 232 (2005) 102–107.
[24] H. Otsuka, K. Kim, A. Kouzu, I. Takimoto, H. Fujimori, Y. Sakata, H. Imamura, T. Matsumoto, K. Toda, Chem. Lett. 34 (2005) 822–823.
[25] Y. Miseki, H. Kato, A. Kudo, Chem. Lett. 35 (2006) 1052–1053.
[26] Y. Miseki, H. Kato, A. Kudo, Energy Environ. Sci. 2 (2009) 306–314.
[27] J. Tang, A.J. Cowan, J.R. Durrant, D.R. Klug, J. Phys. Chem. C 115 (2011) 3143–3150.
[28] A. Mukherji, C. Sun, S.C. Smith, G.Q. Lu, L. Wang, J. Phys. Chem. C 115 (2011) 15674–15678.
[29] S. Chen, J. Yang, C. Ding, R. Li, S. Jin, D. Wang, H. Han, F. Zhang, C. Li, J. Mater. Chem. A 1 (2013) 5651–5659.
[30] Y. Negishi, M. Mizuno, M. Hirayama, M. Omatoi, T. Takayama, A. Iwase, A. Kudo, Nanoscale 5 (2013) 7188–7192.
[31] Y. Negishi, Y. Matsuura, R. Tomizawa, W. Kurashige, Y. Niihori, T. Takayama, A. Iwase, A. Kudo, J. Phys. Chem. C 119 (2015) 11224–11232.
[32] S. Li, W. Cao, C. Wang, H. Qiu, J. Alloy. Compd. 644 (2015) 757–762.
[33] N.C. Hildebrandt, J. Soldat, R. Marschall, Small 11 (2014) 2051–2057.
[34] M. Zhou, X.W. Lou, Y. Xie, Nano Today 8 (2013) 598–618.
[35] Y. Sun, S. Gao, Y. Xie, Chem. Soc. Rev. 43 (2014) 530–546.
[36] J. Low, S. Cao, J. Yu, S. Wageh, Chem. Commun. 50 (2014) 10768–10777.
[37] S. Ida, T. Ishihara, J. Phys. Chem. Lett. 5 (2014) 2533–2542.
[38] T.G. Xu, C. Zhang, X. Shao, K. Wu, Y.F. Zhu, Adv. Funct. Mater. 16 (2006) 1599–1607.
[39] S. Park, H.J. Song, C.W. Lee, S.W. Hwang, I.S. Cho, ACS Appl. Mater. Inter 7 (2015) 21860–21867.
[40] V.J. Babu, S. Vempati, T. Uyar, S. Ramakrishna, Phys. Chem. Chem. Phys. 17 (2015) 2960–2986.
[41] P.E. Blöchl, Phys. Rev. B 50 (1994) 17953–17979.
[42] G. Kresse, D. Joubert, Phys. Rev. B 59 (1999) 1758–1775.
[43] J.P. Perdew, J.A. Chevary, S.H. Vosko, K.A. Jackson, M.R. Pederson, D.J. Singh, C. Fiolhais, Phys. Rev. B 46 (1992) 6671–6687.
[44] J. Heyd, G.E. Scuseria, M. Ernzerhof, J. Chem. Phys. 118 (2003) 8207–8215.
[45] J. Paier, M. Marsman, K. Hummer, G. Kresse, I.C. Gerber, J.G. Ángyán, J. Chem. Phys. 124 (2006) 154709.
[46] A. Jain, G. Hautier, S.P. Ong, C.J. Moore, C.C. Fischer, K.A. Persson, G. Ceder, Phys. Rev. B 84 (2011) 045115.
[47] V.M. Goldschmidt, Skr. Norske Vidensk.-Akad. Oslo, Mat.-Naturvidensk. Kl., 8, 1926.
[48] M.R. Filip, G.E. Eperon, H.J. Snaith, F. Giustino, Nat. Commun. (2014), http://dx.doi.org/10.1038/ncomms6757.
[49] R. Shannon, Acta Crystallogr. A 32 (1976) 751–767.
[50] F. Wang, I. Grinberg, A.M. Rappe, Appl. Phys. Lett. 104 (2014) 152903.
[51] D. Mekam, S. Kacimi, M. Djermouni, M. Azzouz, A. Zaoui, Results Phys. 2 (2012) 156–163.
[52] A. Amat, E. Mosconi, E. Ronca, C. Quarti, P. Umari, M.K. Nazeeruddin, M. Grätzel, F. De Angelis, Nano Lett. 14 (2014) 3608–3616.
[53] T.J. Jacobsson, M. Pazoki, A. Hagfeldt, T. Edvinsson, J. Phys. Chem. C 119 (2015) 25673–25683.
[54] P. Liu, J. Nisar, R. Ahuja, B. Pathak, J. Phys. Chem. C 117 (2013) 5043–5050.
[55] J. Nisar, B. Pathak, R. Ahuja, Appl. Phys. Lett. 100 (2012) 181903.
[56] H.L. Zhuang, R.G. Hennig, J. Phys. Chem. C 117 (2013) 20440–20445.
[57] A. Kiejna, V.V. Pogosov, Phys. Rev. B 62 (2000) 10445–10450.

[58] A. Jain, S.P. Ong, G. Hautier, W. Chen, W.D. Richards, S. Dacek, S. Cholia, D. Gunter, D. Skinner, G. Ceder, K.A. Persson, APL Mater. 1 (2013) 011002.
[59] W. Wunderlich, J. Nucl. Mater. 389 (2009) 57–61.

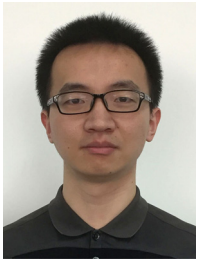

Dihua Wu was born in Hunan, China in 1990. He received his bachelor's degree in Nankai University in 2012. He is pursuing his Ph.D in Nankai University, majoring in inorganic chemistry. Now his research interest mainly focuses on exploring energy storage and conversion materials with both experimental and computational methods.

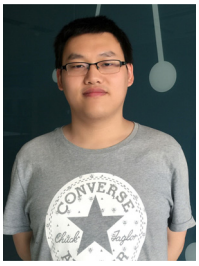

Xu Zhang was born in Shandong, China in 1992. He obtained his bachelor's degree in chemistry at Nankai University in 2014. He has been studying for his Ph.D degree at Nankai University with Professor Zhen Zhou. His research interest mainly focuses on computational study of 2D materials for energy storage and conversion.

Yu Jing was born in Heilongjiang, China in 1988. She received her bachelor's degree in materials chemistry at Nankai University in 2011. Then she joined Prof. Zhou's group and obtained her Ph.D degree in inorganic chemistry at Nankai University in 2016. Her main research interest is 2D materials for energy storage and conversion from the views of experiments and computations.

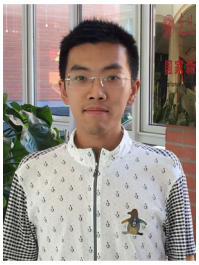

Xudong Zhao was born in Tianjin, China in 1990. He received his bachelor's degree in chemistry at Nankai University in 2013. He has been studying for his Ph.D at Nankai University with Professor Zhen Zhou and his research direction is computational materials science.

Zhen Zhou was born in Shandong, China in 1971. After he received his BSc in 1994 and Ph.D in 1999 at Nankai University, China, he joined the faculty in 1999. Two years later, he began to work at Nagoya University, Japan as a JSPS postdoctoral fellow. In 2005, he returned to Nankai University as an associate professor. In 2011, he was promoted as a full professor. He is now the Director of Computational Center for Molecular Science and Institute of New Energy Material Chemistry, Nankai University. His main research interest is design, preparation and application of advanced materials for energy storage and conversion.